Characterizing the origin of excess dissolved organic carbon in coastal seawater using stable carbon isotope and light absorption characteristics

Heejun Han[1], Jeomshik Hwang[1], Guebuem Kim[1]

[1]School of Earth and Environmental Sciences/Research Institute of Oceanography, Seoul National University, Seoul, 08826, South Korea

Correspondence to: Guebuem Kim (gkim@snu.ac.kr)

Abstract. In order to determine the origins of dissolved organic matter (DOM) occurring in coastal seawater of the Sihwa Lake, South Korea, which is semi-enclosed by a dyke, we measured the stable carbon isotopic ratio of dissolved organic carbon (DOC- $\delta^{13}C$) and optical properties (absorbance and fluorescence) of the DOM in two different seasons (March 2017 and September 2018). The concentrations of DOC were generally higher in lower-salinity waters in both periods, while a significant excess of DOC was observed in 2017 in the same salinity range. The main source of DOC, dependent on salinity, was found to be from marine sediments in the freshwater-seawater mixing zone rather than from terrestrial sources based on the DOC-$\delta^{13}C$ values ($-20.7\pm1.2‰$) and good correlations among DOC, humic-like fluorescent DOM (FDOM$_H$), and NH$_4^+$ concentrations. However, the excess DOC observed in 2017 seems to originate from terrestrial sources by direct land-seawater interactions rather than from in-situ biological production, considering the lower DOC-$\delta^{13}C$ values ($-27.8‰$ to $-22.6‰$) and higher spectral slope ratio (S_R) of light absorbance, without increases in FDOM$_H$ and NH$_4^+$ concentrations. This terrestrial DOM source could have been exposed to light and bacterial degradation for a long time, resulting in nonfluorescent and low-molecular-weight DOM, as this study area is surrounded by the reclaimed land. Our results suggest that the combination of these biogeochemical tools can be a powerful tracer of coastal DOM sources.

1 Introduction

Dissolved organic carbon (DOC), a major component of dissolved organic matter (DOM), is one of the most dominant reduced carbon compounds in the ocean (Benner et al., 1992; Raymond and Spencer, 2014). Understanding of sources and characteristics of DOC is important since it plays a significant role in coastal carbon dynamics and biogeochemical cycles (Vetter et al., 2007; Carson and Hansell, 2015). In the coastal oceans, DOM sources are diverse including (1) in-situ biological production (Carlson and Hansell, 2015), (2) terrestrial sources such as soils and plant matters (Opsahl and Benner, 1997; Bauer and Bianchi, 2011), and (3) anthropogenic sources including industrial and agricultural wastewater (Tedetti et al., 2010; Griffith and Raymond, 2011).

30 A part of DOM is known as colored dissolved organic matter (CDOM), which is the light-absorbing fraction of reduced organic matter (Coble, 2007; Kim and Kim, 2016; Kim and Kim, 2018). The major fraction of CDOM, which is fluorescent after absorbing energy, is referred to as fluorescent DOM (FDOM) (Coble, 2007; Kim and Kim, 2016). Rivers are known as the major source of the humic-like FDOM ($FDOM_H$) in coastal oceans (Stedmon and Nelson, 2015; Kim and Kim, 2016), while aerobic microbial remineralization of sinking organic matter is the major source of $FDOM_H$ in deep oceans (Jørgensen

35 et al., 2011; Catalá et al., 2015; Kim and Kim, 2016). Recently, the anaerobic process in the bottom sediment has also been suggested as an important source of $FDOM_H$ in coastal marine environment (Kim and Kim, 2018). On the other hand, Kim and Kim (2016) showed that the anaerobic production in the bottom sediments of the deep East Sea (Japan Sea) accounted for about 10% of the total production of $FDOM_H$ in the deep water column. In order to obtain such information on FDOM, an excitation-emission matrix (EEM) spectroscopy method combined with a parallel factor analysis (PARAFAC) model has

40 been employed (Coble, 2007; Kim and Kim, 2016; Kim and Kim 2018). In addition, the absorption spectral slope ratio (S_R) can be used as an indicator of molecular weight, source, and photochemistry of DOM since the absorption spectra and spectral parameters for CDOM are largely dependent on its source and photochemical processes (Helms et al., 2008). In general, the S_R values negatively correlate with DOM molecular weight and increase upon irradiation (Helms et al., 2008; Hansen et al., 2016).

45

The stable carbon isotopic composition of DOC (DOC-δ^{13}C) has been used to differentiate terrestrial versus marine DOC (Gearing, 1988; Wang et al., 2004; Lee and Kim, 2018; Lee et al., 2020). In general, δ^{13}C values of terrestrial sources such as C_3 and C_4 plants are in the range of –23‰ to –34‰ and –9‰ to –17‰, respectively, while those derived from marine phytoplankton are in the range of –18‰ to –22‰ (Gearing, 1998). Since δ^{13}C values are likely to overlap within the isotopic

50 ranges, it is hard to differentiate specific carbon source itself. Thus, many of studies used δ^{13}C values combined with other parameters such as optical properties and DOC to dissolved organic nitrogen (DON) ratios to identify different sources of DOM in coastal environments (Lee and Kim, 2018; Han et al., 2020; Lee et al., 2020).

In this study, we used DOC-δ^{13}C combined with FDOM and S_R values to characterize different sources of DOM in Sihwa,

55 Korea. This region is known for one of the most dynamic coastal settings in terms of salinity changes, hypoxia, metal pollution, and eutrophication (Kim et al., 2009; Ra et al., 2011; Lee et al., 2014; Kim and Kim, 2014; Lee et al., 2017; Kim and Kim, 2018).

2 Materials and methods

2.1 Study area and sampling

60 Sihwa (126.6 °E; 37.3 °N) is a reclaimed land with an area of 57 km^2 and average depth of 3.2 m, located on the western coast of South Korea, which was used to build a tidal power plant (Lee et al., 2014) (Fig. 1). The total volume of the Sihwa

Lake water is ~3.3×10⁸ m³ y⁻¹ and the discharge rate is approximately 3.4×10⁸ m³ y⁻¹ (Lee et al., 2014). Sihwa Lake was originally planned to supply agricultural water during the 1980s and 1990s, creating a large artificial lake and agricultural reclaimed land with an area of 173 km² (Bae et al., 2010). There are continuous inputs of anthropogenic pollutants from the

65 surrounding industrial complexes (Lee et al., 2017). Freshwater runs through the six small streams into the Sihwa Lake and four waterways connect the lake to the Banwol industrial complex (Fig. 1). Since the lake experienced serious deterioration of water quality, the sluice gates were opened periodically for the water exchange between the lake and the Yellow Sea since 2012.

70 Water samples were collected in March 2017 and September 2018. The temperature and salinity were measured using a conductivity-temperature-depth (CTD) instrument (Ocean Seven 304, INDONAUT Srl) onboard a ship. In 2018, only surface water samples were collected at shallow stations (station number 1–6) since the water level of the reservoir was lower than in 2017, and the full depth sampling was conducted at stations 12–14. In 2017, sampling was conducted from several depths at all stations. In order to check the effect of industrial wastewater from the industrial complex, an additional

75 sample was collected near the Banwol waterway (station B4) in 2018 (Fig. 1).

Water samples were filtered through a pre-combusted (450 °C for 5h) GF/F filter (pore size: 0.7 μm; Whatman). Samples for DOC and DOC-δ^{13}C analyses were acidified with 6M of HCl to avoid any bacterial activities and stored in pre-combusted glass ampoules. Samples for FDOM analysis were stored in pre-combusted amber vials in a refrigerator at 4°C. Samples for

80 total dissolved nitrogen (TDN) and dissolved inorganic nitrogen (DIN) analyses were stored frozen in a polypropylene conical tube.

2.2 Chemical analyses

Inorganic and organic nutrients were measured with a nutrient auto-analyzer (QuAAtro39, SEAL analytical). The analytical uncertainties were <5% for the reference materials for NO_X (KANTO, Japan). The dissolved oxygen (DO) was determined

85 using the Winkler's method (Carpenter, 1965). DOC concentration was measured using a high temperature catalytic oxidation (HTCO) method using a total organic carbon (TOC) analyzer (TOC-V$_{CPH}$, Shimadzu) (Kim and Kim, 2010; Han et al., 2020). Analysis was also conducted for a certified reference material of deep seawater (DSR; 41–45 μM DOC; University of Miami) (Hansell, 2005). The precision of measurement was ±2.2 μM based on multiple analyses. DOC-δ^{13}C values were measured with an isotope ratio mass spectrometer (IRMS; Isoprime, Elementar) connected with a TOC analyzer

90 (Vario TOC cube, Elementar) (Panetta et al., 2008; Troyer et al., 2010). Prior to the analysis, IAEA-CH6 sucrose (δ^{13}C = – 10.45±0.03 ‰), Suwannee River Fulvic Acid (SRFA; δ^{13}C = –27.6±0.12 ‰; International Humic Substances Society) and DSR (δ^{13}C = –21.5±0.1 ‰; University of Miami) were also analyzed to evaluate the accuracy of the measurements (Panetta et al., 2008; Troyer et al., 2010; Han et al., 2020).

2.3 Optical measurements

95   Fluorescence and absorbance spectra of the samples were measured using a spectrophotometer (Aqualog, Horiba). For FDOM analyses, the emission and excitation wavelength ranges were set from 240 to 600 nm and from 250 to 500 nm, respectively, with 3 nm scanning intervals (Han et al., 2020). The PARAFAC analysis for the EEM data was performed using the Solo software. The Raman and Rayleigh scattering signals, inner-filter effect, and blank subtraction were corrected using the Solo software (Han et al., 2020). The PARAFAC results were validated by a split-half analysis and random

100   initialization. The fluorescence intensities of FDOM were normalized with the Raman peak area of water and are presented in Raman Unit (RU) (Lawaetz and Stedmon, 2009).

The PARAFAC model characterized one marine humic-like, one protein-like, and two terrestrial humic-like fluorescent components (Fig. S1). The spectral characteristics of component 1 ($FDOM_H$; Ex/Em = 342/427 nm) and component 3

105   ($FDOM_{H2}$; Ex/Em = 381/493 nm) are known to be associated with the terrestrial humic-like component (Coble 2007). Component 2 ($FDOM_M$; Ex/Em = 297/388 nm) is known to be associated with the marine humic-like component (Coble, 2007). Component 4 ($FDOM_P$; Ex/Em = 282/322 nm) is characterized as a protein-like (tryptophan-like) component, which originates mainly from biological production (Coble, 2007).

110   UV-visible absorption spectra of the samples were measured with a scanning wavelength range of 240–700 nm. The optical indices and parameters of DOM used in this study were prepared as follows. The absorption coefficient was calculated using the following equation:

$$a_\lambda = 2.303 A_\lambda / l \tag{1}$$

where α is the absorption coefficient (m^{-1}), A_λ is the absorbance, and l is the optical path length of the quartz cuvette (m).

115   The S_R was calculated as the ratio of spectral slope of shorter wavelengths ($S_{275–295}$) to longer wavelengths ($S_{350–400}$) (Helms et al., 2008; Han et al., 2020). The spectral slope (S) was calculated using the following equation:

$$a_\lambda = a_{\lambda_{ref}} e^{-S(\lambda-\lambda_{ref})} \tag{2}$$

where α is the Napierian absorption coefficient (m^{-1}), λ is the wavelength, and λ_{ref} is the reference wavelength (Twardowski et al., 2004; Helms et al., 2008).

120   ## 3 Results

In 2017, the vertical distribution of salinity indicated a well-mixed water column (salinity = 28–32) (Fig. 2). Similarly, DO and NH_4^+ concentrations were vertically uniform (Fig. 2). The concentrations of DO and NH_4^+ were in the ranges of 7–13 mg L^{-1} (average = 10.1±2.4 mg L^{-1}) and 0.1–25 μM (average = 8.7±8.1 μM), respectively, in 2017. The DO concentration gradually increased with increasing salinity from the innermost station to the outermost station (Fig. 2). In contrast, the NH_4^+

125   concentration decreased with increasing salinity (Fig. 2). The NH_4^+ concentration showed the lowest values (< 1 μM) from the station 10 to station 13 (Fig. 2).

In 2018, the vertical distribution of salinity gradually increased (salinity = 18–30) along the estuarine gradient (Fig. 2). Especially, low salinity waters (salinity = 18–27) were observed from the innermost station to the station 9 in 2018 (Fig. 2).

130   The concentrations of DO and NH_4^+ were in the ranges of 6–11 mg L^{-1} (average = 8.2±1.6 mg L^{-1}) and 0.4–25 μM (average = 13.1±7.9 μM), respectively, in 2018 (Fig. 2). The relatively low salinity and DO concentrations were likely associated with the increased freshwater input in 2018 (Fig. 2). In 2018, the NH_4^+ concentrations in the outermost stations were lower than the detection limit (Fig. 2). Although the sharp gradients of DO and NH_4^+ concentrations were observed at station 9 in 2017, they occurred near the station 14 in 2018, associated with the expansion of low-salinity water further to outer stations.

135

In 2017, the vertical distribution of DOC concentrations was quite different from those of salinity and DO concentrations (Fig. 2). The concentrations of DOC were in the range of 97–349 μM (average = 184±76 μM). The highest concentrations of DOC were observed in the surface waters at stations 5, 6, 7, 8, 9 and the bottom waters of stations 3 and 5 (Fig. 2). The DOC-δ^{13}C values ranged from –19.2‰ to –27.8‰ (average = –21.8±1.9‰) in 2017 (Fig. 3). The most depleted DOC-δ^{13}C

140   values were found at stations 5, 6, 7, 9, and 10 in the surface water (–24.6±2.1‰) (Fig. 3). The concentration of $FDOM_H$ (terrestrial humic-like component) and $FDOM_M$ (marine humic-like component) were in the ranges of 1.6–4.1 RU (average = 2.3±0.8 RU) and 1.0–2.4 RU (average = 1.5±0.5 RU), respectively, in 2017 (Fig. 3). The concentrations of $FDOM_H$ and $FDOM_M$ were generally higher in the upstream stations (Kim and Kim, 2018) (Fig. 3). The S_R values, indicating DOM molecular weight, were in the range of 0.70–1.76 (average = 1.21±0.20). Higher S_R values were observed in the surface

145   waters at stations 6, 8, 9, and 10 in 2017 (Fig. 3).

In 2018, the concentrations of DOC were in the range of 101–195 μM (average = 130±32 μM). The DOC concentrations gradually decreased with increasing salinity in 2018 (Fig. 2). The DOC-δ^{13}C values ranged from –19.1‰ to –21.5‰ (average = –20.0±0.6‰) (Fig. 3). The concentrations of $FDOM_H$ and $FDOM_M$ were in the ranges of 1.4–5.1 RU (average =

150   1.9±0.9 RU) and 1.4–4.9 RU (average = 2.1±0.9 RU), respectively (Fig. 3). Both $FDOM_H$ and $FDOM_M$ concentrations were higher in 2018 than in 2017. The S_R values were in the range of 0.72–1.08 (average = 0.87±0.10) (Fig. 3). The S_R values were relatively constant at all sampling stations (Fig. 3).

4 Discussion

In 2017 and 2018 sampling periods, higher DOC in low-salinity was associated with lower DO, higher NH_4^+, and higher

155    $FDOM_H$ concentrations, indicating larger contribution of DOC either from terrestrial fresh water or by production in the estuarine mixing zone (Figs. 2 and 3). In addition, in 2017, there was significant excess of DOC concentrations were observed together with lower DOC-δ^{13}C values and higher S_R values, although such excess anomalies were not observed in

2018, there was no significant excess was found (Figs. 2 and 3). This excess DOC could be produced either by in-situ biological production or supply of terrestrial sources by land-seawater interaction since salinity decreases were observed at
160 these stations.

The DOC concentrations exhibited significant correlations against salinity in both periods with different slopes, while the $FDOM_H$ concentrations exhibited a good correlation with salinity with a single slope (Fig. 4). As such, DOC exhibited good correlations with NH_4^+ concentrations in both periods with different slopes, while the $FDOM_H$ concentrations showed a good
165 correlation with NH_4^+ with a single slope (Fig. 5). These results suggest that the main sources of DOC and $FDOM_H$ in this region are associated with freshwater streams and NH_4^+, with extra source inputs of DOC, which is not fluorescent, in 2017. In this study region, Kim and Kim (2018) hypothesized that $FDOM_H$ is produced by anaerobic decomposition of organic matter in bottom sediments in the freshwater-seawater mixing zone, based on good correlations among salinity, NH_4^+, and $FDOM_H$. However, this correlation cannot rule out the main sources of DOC and $FDOM_H$.

170

The lower DOC slope in 2018 showed a conservative mixing pattern commonly observed in the estuarine mixing zone where terrestrial fresh DOC and marine DOC are mixed (Fig. 4a). However, the DOC-$\delta^{13}C$ values ranged from -19.1‰ to -21.5‰ (average = -20.0±0.6‰), falling within the range of marine phytoplankton (-18‰ to -22‰) (Gearing, 1988). There was no significant excess DOC at station B4 where the waterway connects to the Banwol industrial complex (Fig. 2), indicating that
175 anthropogenic source is insignificant. Thus, this isotope trend, together with the correlations among salinity, DOC, NH_4^+, and $FDOM_H$ in 2018, indicates that DOC is mainly from marine sediments by anaerobic bacterial production as suggested by Kim and Kim (2018).

The higher DOC in 2017 can be separated into two groups (Group 1 and Group 2) based on their sampling stations and
180 DOC-$\delta^{13}C$ values (Fig. 4). Group 1 (n=24) includes most of the samples (stations 2, 3, 4, 11, 12, and 13) with a wide range of salinities and DOC concentrations (Fig. 2). Group 2 (n=6) includes surface water samples in the stations 5, 6, 7, 8, 9, and 10 (Fig. 2). The DOC-$\delta^{13}C$ values of Group 1 ranged from -19.2‰ to -23.4‰, which are close to the $\delta^{13}C$ values of marine organisms (-18‰ to -22‰) (Gearing, 1988) (Fig. 3). However, the DOC-$\delta^{13}C$ values of Group 2 ranged from -21.5‰ to -27.8‰, which are close to the $\delta^{13}C$ values of terrestrial C_3 plants (-23‰ to -32‰) (Gearing, 1988), except for station 8 (-
185 21.5‰) (Fig. 4b). Both $FDOM_H$ and $FDOM_M$ concentrations showed no significant excess in Group 2 (Fig. 3). This implies that the excess DOC of Group 2 may have been introduced from terrestrial sources, which is not fluorescent, through direct interaction between the artificial reclaimed land and seawater (Lee et al., 2020).

Then, we examined the light absorption characteristics of DOM in order to further determine the characteristic of DOM. In
190 2017, higher S_R values (1.37±0.3) were observed for the stations belonging to Group 2, while the S_R values of Group 1 (1.17±0.2) were lower than Group 2 (Fig. 3). In general, S_R values are negatively correlated to molecular weight of DOM

and increase on irradiation (Helms et al., 2008). However, the S_R values were relatively low and constant (0.86±0.1) through all stations in 2018 (Fig. 3). Such large variations in S_R values are likely associated with the photodegradation and biological degradation (Moran et al., 2000; Helms et al., 2008). This Group 2 did not show any increases in $FDOM_H$ relative to NH_4^+ or

195 salinity. Thus, the particularly higher S_R values observed in Group 2 in 2017 are likely associated with the low molecular weight DOM (Helms et al., 2008), as terrestrial DOM (based on DOC-δ^{13}C values) went through intense light (producing non-fluorescent DOM) and bacterial degradation.

If only salinity and $FDOM_H$ were used to trace the source of the excess DOC occurring in Group 2, in-situ production of
200 DOC by biological production can be simply regarded as a main source since there were no changes in these parameters. As such, the fresh, terrestrial source could be regarded as a main source of the excess DOC occurring in low-salinity waters since there were good correlations between salinities and DOC or $FDOM_H$. Therefore, our study suggests that the combination of carbon stable isotope, $FDOM_H$, and S_R values is a critical tool to decipher the sources and characteristics of DOM in coastal waters where various DOM sources are present.

205 **5 Conclusions**

The different sources and distributions of DOM were determined in different seasons using various tracers in the Sihwa Lake, South Korea. The main source of DOC in 2018 was found to be produced by marine sediments based on DOC-δ^{13}C values (-21.5‰ to -19.1‰) and significant correlations among DOC, $FDOM_H$, and NH_4^+ concentrations. However, the main sources of excess DOC were separated into two groups in 2017. DOC in Group 1 was found to be produced by in-situ
210 biological production based on DOC-δ^{13}C values (-19.1‰ to -23.4‰) and the relationship with NH_4^+ concentrations. The excess DOC in Group 2 seems to be produced in the reclaimed land since the samples showed depleted DOC-δ^{13}C values (-22.6‰ to -27.8‰) and higher S_R values (1.37±0.3), without increases in $FDOM_H$ and NH_4^+ concentrations. Our results suggest that the combination of these DOM tracers can be successfully used in other coastal waters where the sources and characteristics of DOM are complicated.

215

Data availability. All data are available upon request to the corresponding author.

Author contributions. HH and GK were involved in planning the research. HH collected samples and performed the analyses. All authors were involved in analyzing the results and writing the paper.

220

Competing interests. The authors declare that they have no conflict of interest.

Acknowledgements. This research was supported by the National Research Foundation (NRF) of Korea (NRF-2018R1A2B3001147) funded by the South Korean government. We would like to thank all lab members for their assistance.

225 **References**

Bae, Y. H., Kim, K. O., and Choi, B. H.: Lake Sihwa tidal power plant project, Ocean. Eng., 37, 454–463, https://doi.org/10.1016/j.oceaneng.2010.01.015, 2010.

Bauer, J. E. and Bianchi, T. S.: Dissolved organic carbon cycling and transformation, in: Treatise on estuarine and coastal science, edited by: Wolanski, E. and Mcluski, D. S., 5, 7–67, Academic Press, Waltham, 2011.

230 Benner, R., Pakulski, J. D., McCarthy, M., Hedges, J. I., and Hatcher, P. G.: Bulk chemical characteristics of dissolved organic matter in the ocean, Science, 255, 1561–1564, https://doi.org/10.1126/science.255.5051.1561, 1992.

Carlson, C. A. and Hansell, D. A.: Chapter 3 – DOM sources, sinks, reactivity, and budgets, in: Biogeochemistry of marine dissolved organic matter (Second Edition), edited by: Hansell, D. A. and Carlson, C. A., 65–126, Academic Press, Boston, 2015.

235 Carpenter, J. H.: The Chesapeake Bay institute technique for the Winkler dissolved oxygen method, Limnol. Oceanogr., 10, 141–143, 1965.

Catalá, T. S., Reche, I., Álvarez, M., Khatiwala, S., Guallart, E. F., Benítez-Barrios, V. M., Fuentes-Lema, A., Romera-Castillo, C., Nieto-Cid, M., Pelejero, C., Fraile-Nuez, E., Ortega-Retuerta, E., Marrasé, C., and Álvarez-Salgado, X. A.: Water mass age and aging driving chromophoric dissolved organic matter in the dark global ocean, Global

240 Biogeochem. Cy., 29, 917–934, https://doi.org/10.1002/2014GB005048, 2015.

Coble, P. G.: Marine optical biogeochemistry: the chemistry of ocean color, Chem. Rev., 107, 402–418, https://doi.org/10.1021/cr050350+, 2007.

Gearing, J. N.: The use of stable isotope ratios of tracing the nearshore-offshore exchange of organic matter, in: Coastal-offshore ecosystem interactions, edited by: Jansson, B.-O., 69–101, Springer-Verlag, Berlin, 1988.

245 Griffith, D. R. and Raymond, P. A.: Multiple-source heterotrophy fuelled by aged organic carbon in an urbanized estuary, Mar. Chem., 124, 14–22, https://doi.org/10.1016/j.marchem.2010.11.003, 2011.

Han, H., Kim, G., Seo, H., Shin, K.-H., and Lee, D.-H.: Significant seasonal changes in optical properties of brown carbon in the midlatitude atmosphere, Atmos. Chem. Phys., 20, 2709–2718, https://doi.org/10.5194/acp-20-2709-2020, 2020.

Hansen, A. M., Kraus, T. E. C., Pellerin, B. A., Fleck, J. A., Downing, B. D., and Bergamaschi, B. A.: Optical properties of

250 dissolved organic matter (DOM): Effects of biological and photolytic degradation, Limnol. Oceanogr., 61, 1015–1032, https://doi.org/10.1002/lno.10270, 2016.

Helms, J. R., Stubbins, A., Ritchie, J. D., and Minor, E. C.: Absorption spectral slopes and slope ratios as indicators of molecular weight, source, and photobleaching of chromophoric dissolved organic matter, Limnol. Oceanogr., 53, 955–969, https://doi.org/10.4319/lo.2008.53.3.0955, 2008.

255 Jørgensen, L., Stedmon, C. A., Kragh, T., Markager, S., Middelboe, M., Søndergaard, M.: Global trends in the fluorescence characteristics and distribution of marine dissolved organic matter, Mar. Chem., 126, 139–148, https://doi.org/10.1016/j.marchem.2011.05.002, 2011.

Kim, J. and Kim, G.: Significant anaerobic production of fluorescent dissolved organic matter in the deep East Sea (Sea of Japan), Geophys. Res. Lett., 43, 7609–7616, https://doi.org/10.1002/2016GL069335, 2016.

260 Kim, J. and Kim, T.-H.: Distribution of humic fluorescent dissolved organic matter in lake Shihwa: the role of the redox condition, Estuar. Coast., https://doi.org/10.1007/s12237-018-00491-0, 2018.

Kim, K. T., Kim, E. S., Cho, S. R., and Park, J. K.: Distribution and temporal change of heavy metals in the surface sediments of lake Shihwa and adjacent sea, Korea, J. Coast. Res., 56, 817–821, 2009.

Kim, T.-H. and Kim, G.: Distribution of dissolved organic carbon (DOC) in the southwestern East Sea in summer, Ocean 265 Polar Res., 32, 291–297, 2010.

Kim, T.-H. and Kim, G.: Estimating benthic fluxes of trace elements to hypoxic coastal waters using ^{210}Po, Estuar. Coast. Shelf. Sci., 151, 324–330, https://doi.org/10.1016/j.ecss.2014.05.008, 2014.

Lee, C.-H., Lee, B.-Y., Chang, W. K., Hong, S., Song, S. J., Park, J., Kwon, B., Khim, J. S.: Environmental and ecological effects of Lake Shihwa reclamation project in South Korea: A review, Ocean. Coast. Manage., 102, 545–558, 270 https://doi.org/10.1016/j.ocecoaman.2013.12.018, 2014.

Lee, J., Hong, S., Yoon, S. J., Kwon, B., Ryu, J., Giesy, J. P., Allam, A. A., Al-khedhairy, A. A., and Khim, J. S.: Long-term changes in distributions of dioxin-like and estrogenic compounds in sediments of Lake Sihwa, Korea: Revisited mass balance, Chemosphere, 181, 767–777, https://doi.org/10.1016/j.chemosphere.2017.04.074, 2017.

Lee, S.-A., Kim, T.-H., and Kim, G.: Tracing terrestrial versus marine sources of dissolved organic carbon in a coastal bay 275 using stable carbon isotopes, Biogeosciences, 17, 135–144, https://doi.org/10.5194/bg-17-135-2020, 2020.

Moran, M. A., Sheldon, W. M., and Zepp, R. G.: Carbon loss and optical property changes during long-term photochemical and biological degradation of estuarine dissolved organic matter, Limnol. Oceanogr., 45, 1254–1264, 2000.

Opsahl, S. and Benner, R.: Distribution and cycling of terrigenous dissolved organic matter in the ocean, Nature, 386, 480–482, https://doi.org/10.1038/386480a0, 1997.

280 Panetta, R. J., Ibrahim, M., and Gélinas, Y.: Coupling a high-temperature catalytic oxidation total organic carbon analyzer to an isotope ratio mass spectrometer to measure natural-abundance δ^{13}C-dissolved organic carbon in marine and freshwater samples, Anal. Chem., 80, 5232–5239, https://doi.org/10.1021/ac702641z, 2008.

Ra, K., Bang, J.-H., Lee, J.-M., Kim, K.-T., and Kim, E.-S.: The extent and historical trend of metal pollution recorded in core sediments from the artificial Lake Shihwa, Korea, Mar. Pollut. Bull., 62, 1814–1821, 285 https://doi.org/10.1016/j.marpolbul.2011.05.010, 2011.

Raymond, P. A. and Spencer, R. G. M.: Chapter 11 – Riverine DOM, in: Biogeochemistry of marine dissolved organic matter (Second Edition), edited by: Hansell, D. A. and Carlson, C. A., 509–535, Academic Press, Boston, 2015.

Stedmon, C. A. and Nelson, N. B.: Chapter 10 – The optical properties of DOM in the ocean, in: Biogeochemistry of marine dissolved organic matter (Second Edition), edited by: Hansell, D. A. and Carlson, C. A., 481–508, Academic Press, 290 Boston, 2015.

Tedetti, M., Guigue, C., and Goutx, M.: Utilization of a submersible UV fluorometer for monitoring anthropogenic inputs in the Mediterranean coastal waters, Mar. Pollut. Bull., 60, 350–362, https://doi.org/10.1016/j.marpolbul.2009.10.018, 2010.

Troyer, I. D., Bouillon, S., Barker, S., Perry, C., Coorevits, K., and Merckx, R.: Stable isotope analysis of dissolved organic
295   carbon in soil solutions using a catalytic combustion total organic carbon analyzer-isotope ratio mass spectrometer with a cryofocusing interface, Rapid Commun. Mass Spectrom., 24, 365–374, https://doi.org/10.1002/rcm.4403, 2010.

Twardowski, M. S., Boss, E., Sullivan, J. M., and Donaghay, P. L.: Modeling the spectral shape of absorbing chromophoric dissolved organic matter, Mar. Chem., 89, 69–88, https://doi.org/10.1016/j.marchem.2004.02.008, 2004.

Vetter, T. A., Perdue, E. M., Ingall, E., Koprivnjak, J.-F., and Pfromm, P. H.: Combining reverse osmosis and electrodialysis
300   for more complete recovery of dissolved organic matter from seawater, Sep. Purif. Technol., 56, 383–387, https://doi.org/10.1016/j.seppur.2007.04.012, 2007.

Wang, X.-C., Chen, R. F., and Gardner, G. B.: Sources and transport of dissolved and particulate organic carbon in the Mississippi River estuary and adjacent coastal waters of the northern Gulf of Mexico, Mar. Chem., 89, 241–256, https://doi.org/10.1016/j.marchem.2004.02.014, 2004.

305
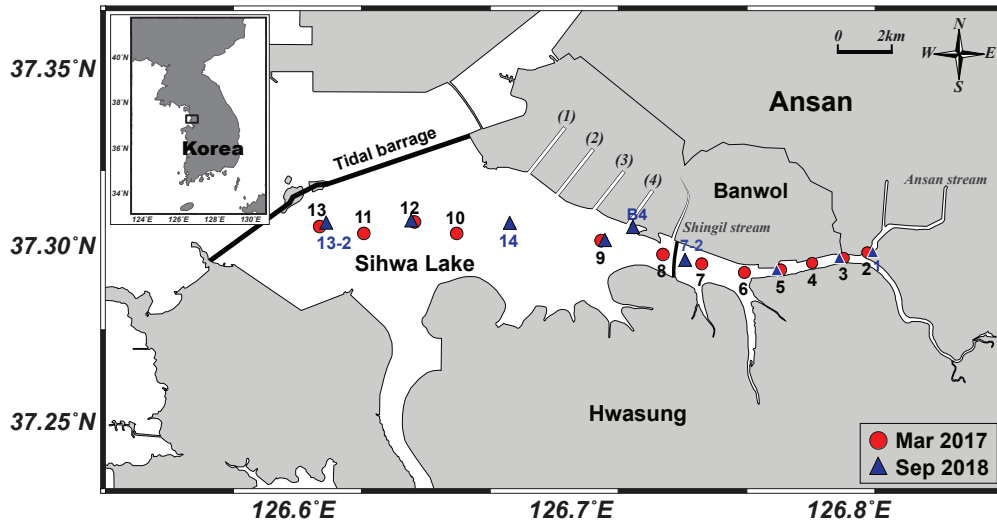
310 **Figure 1: Map of sampling stations in Sihwa, South Korea.**
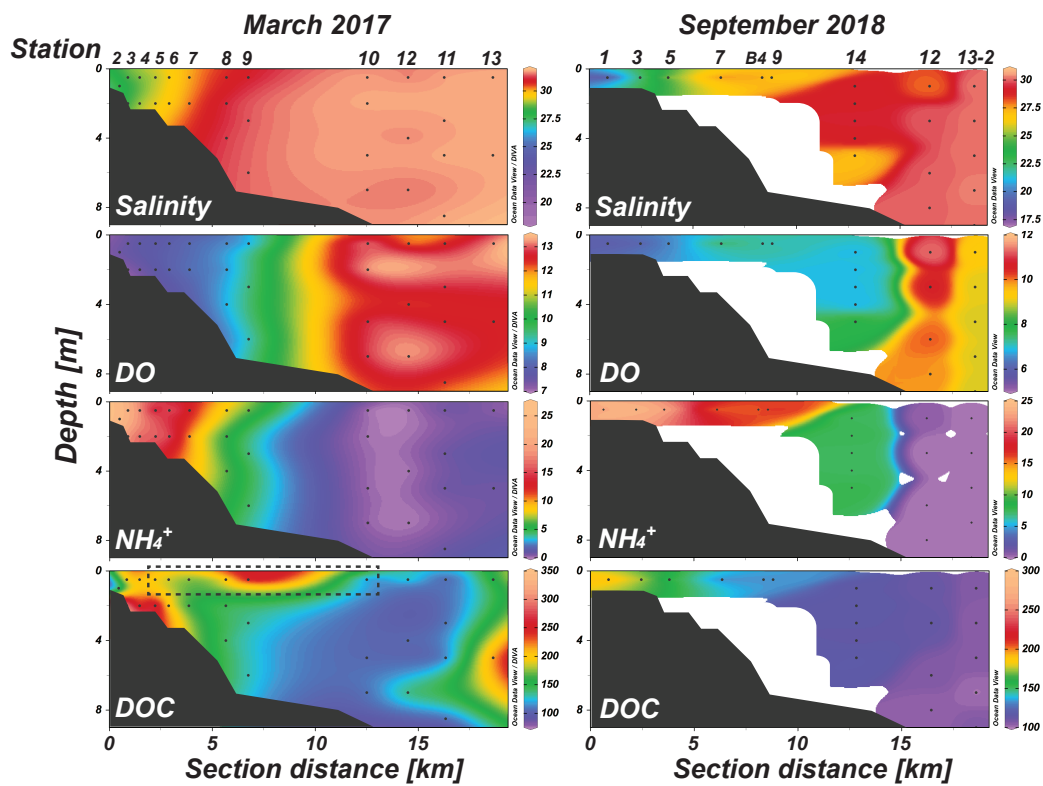
Figure 2: Vertical distributions of salinity, DO, NH$_4^+$, and DOC concentrations in Sihwa in March 2017 and September 2018. The dashed blocks represent stations belonging to Group 2.

315

320
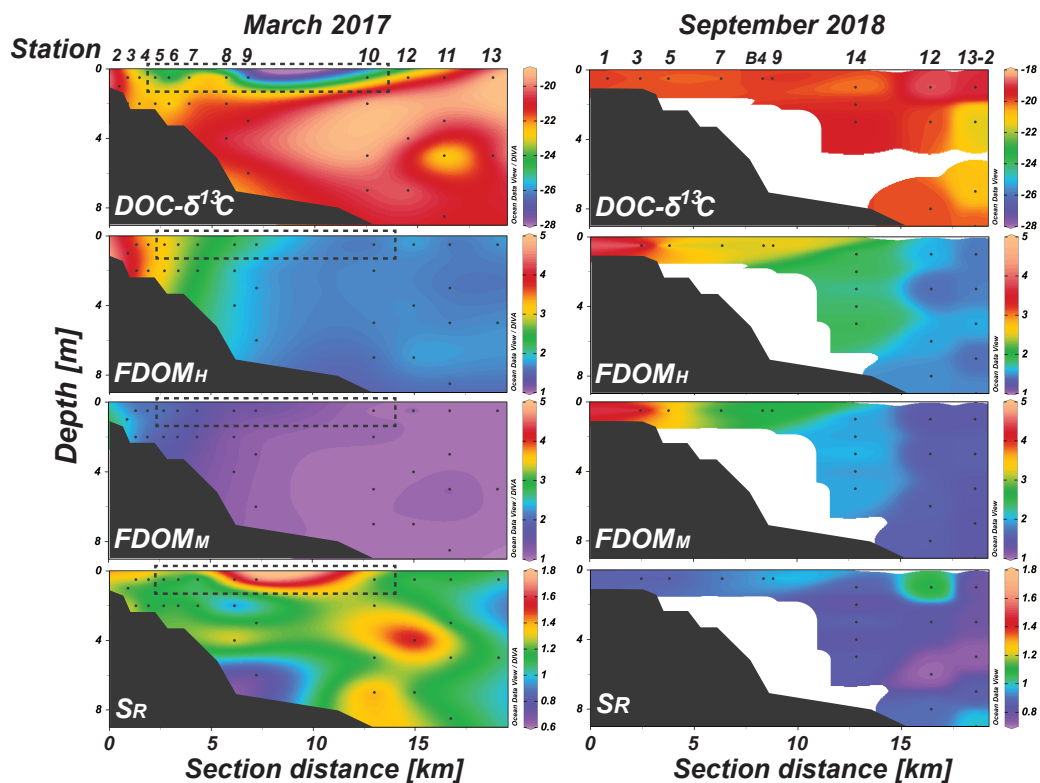
325

Figure 3: Vertical distributions of DOC-δ^{13}C, FDOM$_H$, FDOM$_M$, and S$_R$ values in Sihwa in March 2017 and September 2018. The dashed blocks represent stations belonging to Group 2.

330

335

340
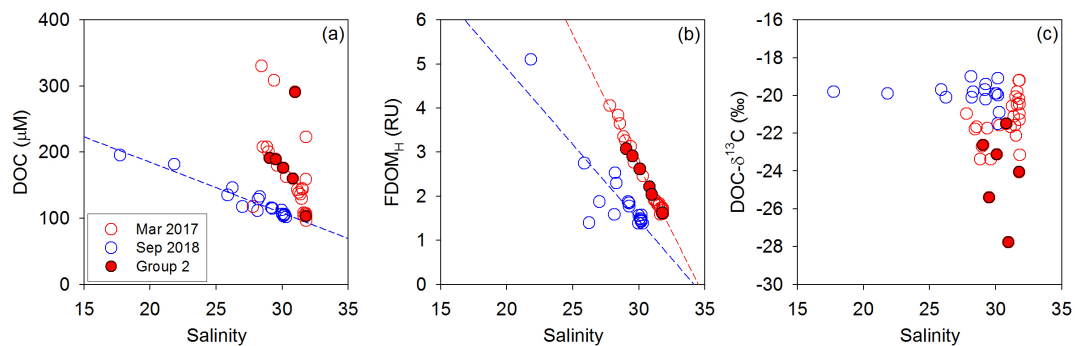
Figure 4: Plots of the salinity versus (a) DOC concentrations, (b) FDOM$_H$ concentrations, and (c) DOC-δ^{13}C values in Sihwa in March 2017 (red) and September 2018 (blue). The dashed lines represent the regression lines and the closed circles (red) represent sample in Group 2.

350

355

360

365

370

375
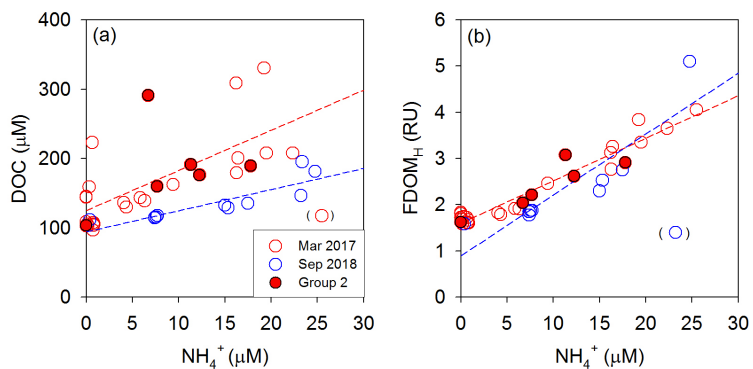
Figure 5: Plots of the NH$_4^+$ concentrations versus (a) DOC concentrations and (b) FDOM$_H$ concentrations in March 2017 (red) and September 2018 (blue). The dashed lines represent the regression lines and the closed circles (red) represent sample in Group 2.

380